



Cancer Research

Natural Killer Cells Eradicate Galectin-1–Deficient Glioma in the Absence of Adaptive Immunity

Gregory J. Baker, Peter Chockley, Viveka Nand Yadav, et al.

Cancer Res Published OnlineFirst July 18, 2014.

Updated version	Access the most recent version of this article at: doi: 10.1158/0008-5472.CAN-14-1203
Supplementary Material	Access the most recent supplemental material at: http://cancerres.aacrjournals.org/content/suppl/2014/07/23/0008-5472.CAN-14-1203.DC1.html

E-mail alerts [Sign up to receive free email-alerts](#) related to this article or journal.

Reprints and Subscriptions To order reprints of this article or to subscribe to the journal, contact the AACR Publications Department at pubs@aacr.org.

Permissions To request permission to re-use all or part of this article, contact the AACR Publications Department at permissions@aacr.org.

Natural Killer Cells Eradicate Galectin-1–Deficient Glioma in the Absence of Adaptive Immunity

Gregory J. Baker^{1,2}, Peter Chockley^{1,2}, Viveka Nand Yadav^{1,2}, Robert Doherty^{1,2}, Michael Ritt², Sivaraj Sivaramakrishnan^{2,3}, Maria G. Castro^{1,2}, and Pedro R. Lowenstein^{1,2}

Abstract

Natural killer (NK) cells safeguard against early tumor formation by destroying transformed target cells in a process referred to as NK immune surveillance. However, the immune escape mechanisms used by malignant brain tumors to subvert this innate type of immune surveillance remain unclear. Here we show that malignant glioma cells suppress NK immune surveillance by overexpressing the β -galactoside-binding lectin galectin-1. Conversely, galectin-1–deficient glioma cells could be eradicated by host NK cells before the initiation of an antitumor T-cell response. *In vitro* experiments demonstrated that galectin-1–deficient GL26-Cit glioma cells are ~3-fold more sensitive to NK-mediated tumor lysis than galectin-1–expressing cells. Our findings suggest that galectin-1 suppression in human glioma could improve patient survival by restoring NK immune surveillance that can eradicate glioma cells. *Cancer Res*; 74(18); 1–12. ©2014 AACR.

I may not have gone where I intended to go, but I think I have ended up where I needed to be.

–Douglas Adams

Introduction

Natural killer (NK) cells represent the main effector lymphocytes of the innate immune system (1, 2). These cells guard against early tumor formation by eliminating transformed cells through NK immune surveillance. NK cells interpret signals on tumor (or virally infected) cells, such as reduced major histocompatibility complex I (MHC-I) expression, as a sign of non-self and/or malignant transformation and lyse such cells when in the context of certain costimulatory molecules (3, 4). The mechanisms used by malignant brain tumors, such as glioblastoma (GBM), to escape NK-mediated immune surveillance remain poorly understood.

Galectin-1 (gal-1) is a member of a family of β -galactoside-binding lectins. Increased gal-1 expression is detected in primary human prostate, colorectal, bladder, pancreatic, liver, thyroid, ovarian, uterine, cervical, and brain cancers, where its expression

is correlated with worse histological grade and poor patient prognosis (5–14). Because it was first shown that cell surface gal-1 induces apoptosis in cytotoxic T cells (15), it has been proposed that this represents the primary mechanism by which tumor-derived gal-1 suppresses antitumor immunity (16–21).

Here we report that shRNA-mediated gal-1 knockdown in glioma cells leads to the rapid accumulation of cytotoxic NK cells within the brain tumor microenvironment that culminates in complete tumor eradication in the absence of an antitumor T-cell response. The suppression of glioma-derived gal-1 is predicted to translate into novel therapies for human malignant gliomas by heightening innate antitumor NK immune surveillance.

Materials and Methods

Animal strains

Six- to 7-week-old female C57BL/6J, B6.129S7-*Rag1*^{tm1Mom}/J (i.e., *RAG1*^{−/−}), and NOD.Cg-*Prkdc*^{scid}*Il2rg*^{tm1Wjl}/SzJ (i.e., NOD-*scid* *IL2Rg*^{null} or NSG) mice were purchased from Jackson Laboratory. LEW/SsNHsd Lewis rats (200–240 g) were purchased from Harlan Laboratories. All animal experiments were conducted in accordance with procedures approved by the University Committee on Use and Care of Animals and conformed to the policies and procedures of the Unit for Laboratory Animal Medicine at the University of Michigan.

Cell lines and culture conditions

GL26-Cit, CNS-1-Cit, GL26-Cit-NT, GL26-Cit-EV, CNS-1-Cit-NT, GL26-Cit-galIi, and CNS-1-Cit-galIi were cultured *in vitro* under humidified conditions in 95% air/5% CO₂ at 37°C. Culture medium for mCitrine⁺ glioma cell lines consisted of Dulbecco's Modified Eagle Medium (DMEM) supplemented with 10% heat-inactivated fetal bovine serum (FBS), 0.3 mg/mL L-glutamine, 50 U/mL penicillin, 50 μ g/mL streptomycin, and 6 μ g/mL G418 selection antibiotic (for selection of the mCitrine expression vector) and were passaged every 2 to 4 days. In addition to the above reagents, GL26-Cit-NT, GL26-Cit-EV,

¹Department of Neurosurgery, University of Michigan Medical School, Ann Arbor, Michigan. ²Department of Cell and Developmental Biology, University of Michigan Medical School, Ann Arbor, Michigan. ³Department of Biomedical Engineering, University of Michigan, Ann Arbor, Michigan.

Note: Supplementary data for this article are available at Cancer Research Online (<http://cancerres.aacrjournals.org/>).

G.J. Baker is a doctoral candidate in the Department of Molecular and Medical Pharmacology, David Geffen School of Medicine, University of California, Los Angeles, Los Angeles, CA.

Corresponding Author: Pedro R. Lowenstein, MSRB II, Room 4570, University of Michigan School of Medicine, 1150 West Medical Center Drive, Ann Arbor, MI 48109-5689. Phone: 734-764-0851; Fax: 734-764-7051; E-mail: pedrol@umich.edu

doi: 10.1158/0008-5472.CAN-14-1203

©2014 American Association for Cancer Research.

CNS-1-Cit-NT, GL26-Cit-gal1i, and CNS-1-Cit-gal1i cells were also cultured in the presence of 3 $\mu\text{g}/\text{mL}$ of puromycin selection antibiotic to select for shRNA expression vectors.

Engineering GL26-Cit, CNS-1-Cit, and their respective gal-1-deficient and control shRNA cell lines

The plasmid containing the mCitrine transgene (pRSET-B-Citrine) was subcloned into the pCI-neo expression vector backbone to afford a 6,199 base-pair plasmid to constitutively express mCitrine fluorescent protein (pCI-neo-mCitrine; Supplementary Fig. S1). This plasmid was then used to transfect both wild-type GL26 and CNS-1 cells. Transfected cells were sorted for high mCitrine expression by FACS and cultured under G418 selection antibiotic to maintain transgene expression.

To establish the GL26-Cit-gal1i and CNS-1-Cit-gal1i cell lines, several pLKO.1-puro lentiviral plasmids encoding both a puromycin resistance cassette and an shRNA hairpin construct specific for rodent galectin-1 (*mlgals1*, NM_008495) mRNA were purchased from Sigma-Aldrich as part of the RNAi consortium. Each shRNA clone was tested for its ability to knockdown gal-1 expression. To do so, a rodent galectin-1 overexpression vector pCMV6-kan/neo-mlgals1 (Origene, cat. no. MC200092) was cotransfected into HEK293 cells along with each of the aforementioned shRNA constructs. RNAi consortium clone TRCN0000011866 afforded the highest level of gal-1 knockdown and was used to create a second-generation lentiviral vector encoding this *mlgals1*-specific shRNA (LV-*mLgals1*-11866). GL26-Cit and CNS-1-Cit cells were then transduced

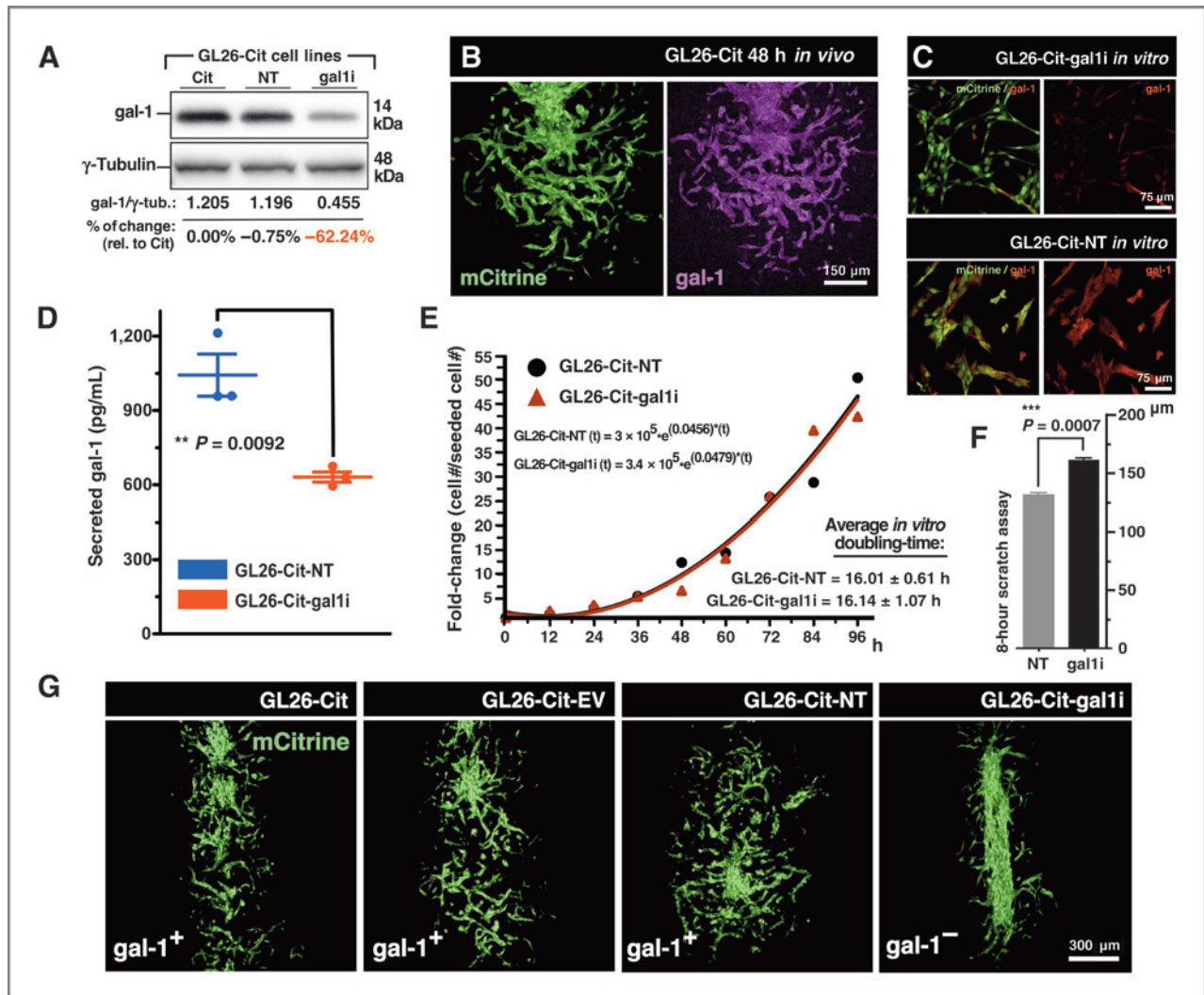
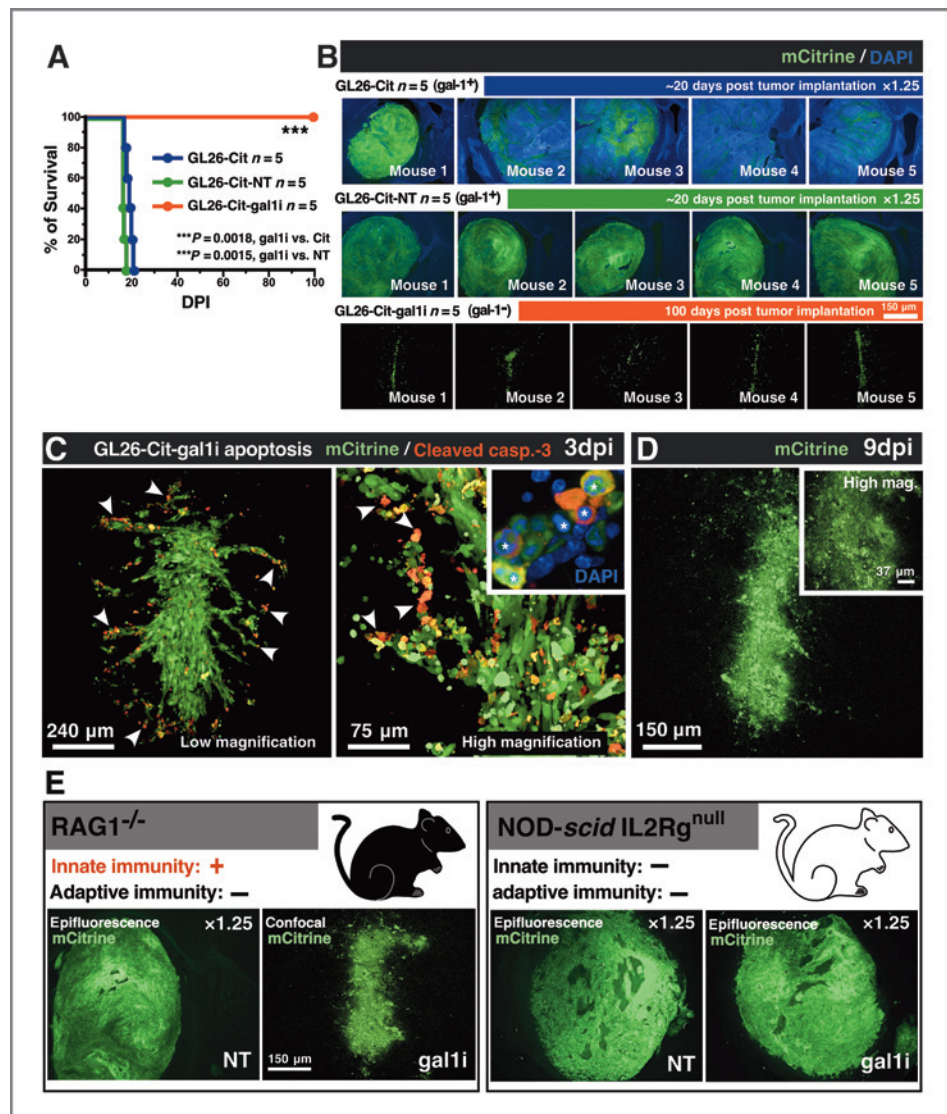


Figure 1. Gal-1 knockdown in mouse GL26-Cit glioma cells. **A**, Western blot analysis for gal-1 in mouse GL26-Cit glioma. GL26-Cit (Cit), GL26-Cit-NT (NT), and GL26-Cit-gal1i (gal1i). **B**, confocal micrograph of GL26-Cit glioma immunolabeled with anti-gal-1 antibodies (magenta) after 48 hours in the RAG1^{-/-} mouse striatum. **C**, immunocytochemistry for gal-1 in GL26-Cit-gal1i cells and GL26-Cit-NT cells. **D**, secreted gal-1 ELISA on GL26-Cit-NT and GL26-Cit-gal1i cells *in vitro* (**, $P = 0.0092$; $1,043 \pm 84.92$ pg/mL NT vs. 631.0 ± 20.30 pg/mL gal1i; unpaired, two-tailed, Student *t* test). **E**, cell growth curve used to calculate average *in vitro* cell doubling times for GL26-Cit-NT and GL26-Cit-gal1i cells over 96 hours *in vitro*. Exponential growth fitting [$r(t) = r_0 e^{kt}$] was applied to estimate respective population doubling times as indicated. **F**, scratch assay assessing the migration rate of GL26-Cit-gal1i cells compared with GL26-Cit-NT *in vitro* over 8 hours. (***, $P = 0.0007$; 130.58 ± 0.92 μm NT vs. 161.49 ± 1.32 μm gal1i; paired, two-tailed, Student *t* test). **G**, confocal micrographs of GL26-Cit tumors 48 hours posttumor implantation into the RAG1^{-/-} striatum.

Figure 2. Gal-1-deficient glioma cells undergo early caspase-3-dependent cell death *in vivo*. **A**, Kaplan–Meier survival analysis of RAG1^{-/-} mice bearing the indicated intracranial GL26-Cit gliomas ($n = 45$; 5 mice/group, study repeated $\times 3$). Mantel–Cox log-rank test detected a highly significant survival difference between GL26-Cit-gal1i and both GL26-Cit (***, $P = 0.0018$) and GL26-Cit-NT (***, $P = 0.0015$) groups. **B**, epifluorescence micrographs of intracranial gliomas (green) corresponding to moribund mice from the survival analysis shown in **A**. Residual mCitrine from GL26-Cit-gal1i tumors (bottom row) 100 dpi was imaged with high-magnification confocal microscopy. **C**, confocal micrographs of GL26-Cit-gal1i tumors immunolabeled with anticleaved caspase-3 after 3 dpi in the RAG1^{-/-} mouse striatum. Condensed/fragmented nuclear chromatin (white asterisks) was visualized with DAPI (blue). White arrowheads indicate several examples of GL26-Cit-gal1i apoptosis. **D**, confocal micrograph of GL26-Cit-gal1i glioma after complete lysis 9 dpi. **E**, representative micrographs of GL26-Cit-NT and GL26-Cit-gal1i gliomas in RAG1^{-/-} and NOD-*scid* IL2Rg^{null} mice.



with 80 μ L of purified LV-*mLgals1*-11866i for 48 to 72 hours. Infected cells were continually grown under puromycin selection to enrich for transduced cells. Similar methodology was used to create the GL26-Cit-NT, GL26-Cit-EV, and CNS-1-Cit-NT control cell lines, which also contain the pLKO.1-puro lentiviral expression vector, but either express a non-targeting shRNA hairpin construct (Mission shRNA, cat. no. SHC002; Sigma-Aldrich) or no shRNA insert (empty expression vector; Mission shRNA, cat. no. SHC001; Sigma-Aldrich).

Primary antibodies used for immunohistochemistry and SDS–PAGE Western blot analysis

Purified goat polyclonal anti-mouse galectin-1 (5 μ g/mL), cat. no. AF1245, R&D Systems; purified rabbit polyclonal anticleaved caspase-3 (Asp 175), (1:300), cat. no. 9661; Cell Signaling Technology; purified hamster anti-mouse CD49b (DX5), (1:500), cat. no. 103507, BioLegend; purified rat anti-mouse Nkp46 (29A1.4), (1:500), cat. no. 560754, BD Pharmingen; FITC-conjugated mouse anti-granzyme B (GB11), (1:1,000), cat.

no. 515403, BioLegend; purified Armenian hamster anti-mouse CD3e (145–2C11), (1:500), cat. no. 553057, BD Pharmingen. Note: no surfactants or antigen retrieval steps were used in any NK cell or T-cell immunolabeling procedure. Detailed immunohistochemical and SDS-PAGE Western blot methodology can be found in the Supplementary Experimental Procedures section available online.

Stereotactic tumor implantation and processing of tissue samples

We have previously described the procedure for stereotactic intracranial tumor implantation into the rodent brain (22). A brief description of the stereotactic tumor implantation and transcatheter perfusion procedures can be found in the Supplementary Experimental Procedures section available online.

In vivo immunodepletion studies

The following antibodies were administered intraperitoneally to deplete NK cells or basophils; per mouse: 25 μ L of stock rabbit

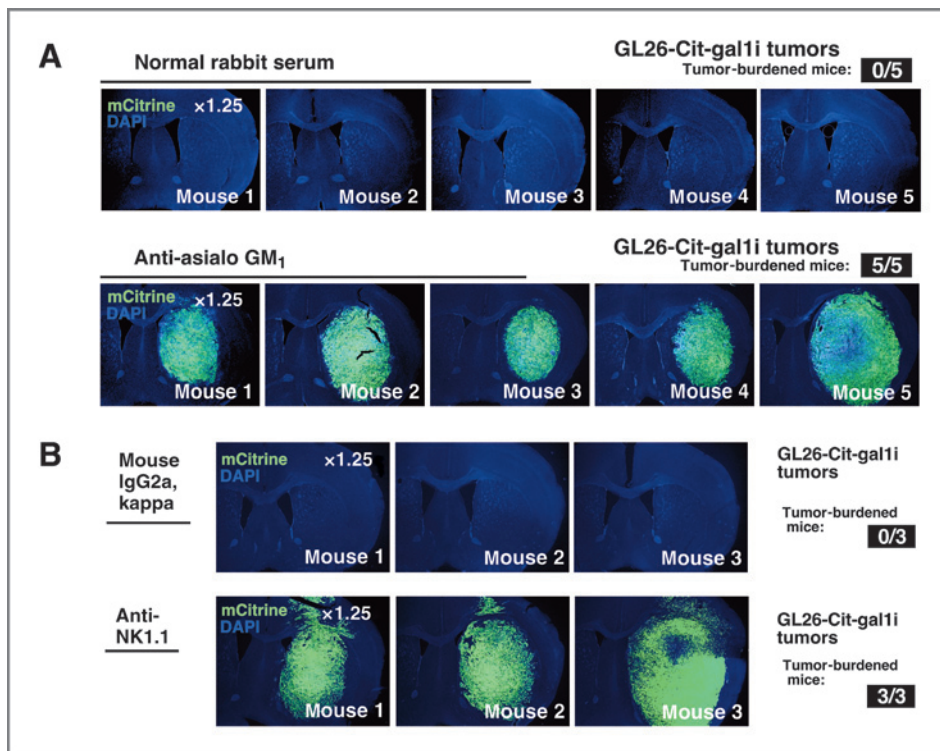


Figure 3. Immunodepletion of NK cells permits gal-1-deficient glioma growth in $RAG1^{-/-}$ mice. **A**, NK-cell depletion with anti-asialo GM₁ in $RAG1^{-/-}$ mice bearing GL26-Cit-gal1i cells after 16 dpi. Top epifluorescence micrographs show the brains of five control mice. Bottom epifluorescence micrographs show the brains of five mice treated with NK-depleting anti-asialo GM₁ ($n = 20$; five mice/treatment group; study repeated 2 \times ; results from one study shown). **B**, NK-cell depletion with anti-NK1.1 monoclonal antibodies in $RAG1^{-/-}$ mice bearing GL26-Cit-gal1i cells after 16 dpi. Top epifluorescence micrographs show the brains of three control mice. Bottom epifluorescence micrographs show the brains of three mice treated with anti-NK1.1 ($n = 6$; three mice/treatment group).

polyclonal anti-asialo GM₁, cat. no. 986-10001, Wako, diluted to a final volume of 100 μ L in ddH₂O administered 1 day before and after tumor implantation, then every 3 days; 100 μ L of undiluted normal rabbit serum (NRS), cat. no. 16120, Life Technologies, administered 1 day before and after tumor implantation then every 3 days; 200 μ g of mouse monoclonal anti-NK1.1 functional grade purified (clone:PK136), cat. no. 16-5941, eBioscience diluted to a final volume of 400 μ L in sterile Dulbecco's Phosphate Buffered Saline (DPBS) pH 7.4 and administered 2 days before tumor implantation and every 4 days; 400 μ L (equivalent to 200 μ g) of undiluted purified mouse IgG2a, κ isotype control antibody (clone:MG2a-53), cat. no. 401502, BioLegend, administered 2 days before tumor implantation and every 4 days; 300 μ L (equivalent to 30 μ g) of undiluted rat monoclonal anti-CD200R3 (clone:ba103), cat. no. HM1103, Hycult Biotech, administered 1 day before tumor implantation and every 5 days; 30 μ L (equivalent to 30 μ g) of purified rat IgG2b, κ isotype control antibody (clone:RTK4530), cat. no. 400637, BioLegend, diluted to a final volume of 300 μ L in 0.9% NaCl administered 1 day before tumor implantation and every 5 days.

Antibodies used for flow cytometry

NK cells were isolated using mouse monoclonal APC-conjugated NK1.1 (PK136), cat. no. 17-5941-82, eBioscience; and Syrian hamster pacific blue-conjugated CD3e (500A2), cat. no. 558214, BD Pharmingen. Glioma-infiltrating NK cells were analyzed using PE-conjugated rat anti-mouse CD45 (30F11), cat. no. 553081, BD Pharmingen; APC-conjugated mouse anti-mouse NK1.1 (PK136), cat. no. 17-5941-82, eBioscience; Pacific blue-conjugated syrian hamster CD3e (500A2), cat. no. 558214, BD Pharmingen; and FITC-conjugated mouse monoclonal anti-granzyme B (GB11), cat. no. 515403, BioLegend. Details on the

harvesting and processing of whole splenocytes and glioma-infiltrating lymphocytes can be found in the Supplementary Experimental Procedures section available online and in ref. 23.

ELISpot

Details on the ELISpot procedure can be found in the Supplementary Experimental Procedures section available online.

Fluorimetry

Details on the fluorimetry procedure can be found in the Supplementary Experimental Procedures section available online.

Statistical analysis

Statistical analyses were performed using GraphPad Prism5 (GraphPad Software, Inc.). Data are reported as mean \pm SEM and were examined with the statistical tests specified in each figure legend. Values were considered significant at the $P \leq 0.05$ level.

Accession numbers

Mouse GL26 brain tumor microarray data are available at the NCBI Gene Expression Omnibus (GEO) database (<http://www.ncbi.nlm.nih.gov/geo/>), accession number GSE11420.

Results

Gal-1 knockdown in mouse GL26-Cit glioma cells causes an *in vivo*-specific growth deficiency

Examination of genome-wide microarray data from mouse GL26 gliomas harvested from the brains of syngeneic C57BL/6 mice (NCBI GEO database, accession GSE11420) revealed that gal-1 (*mGals1*) was the most abundantly expressed mRNA

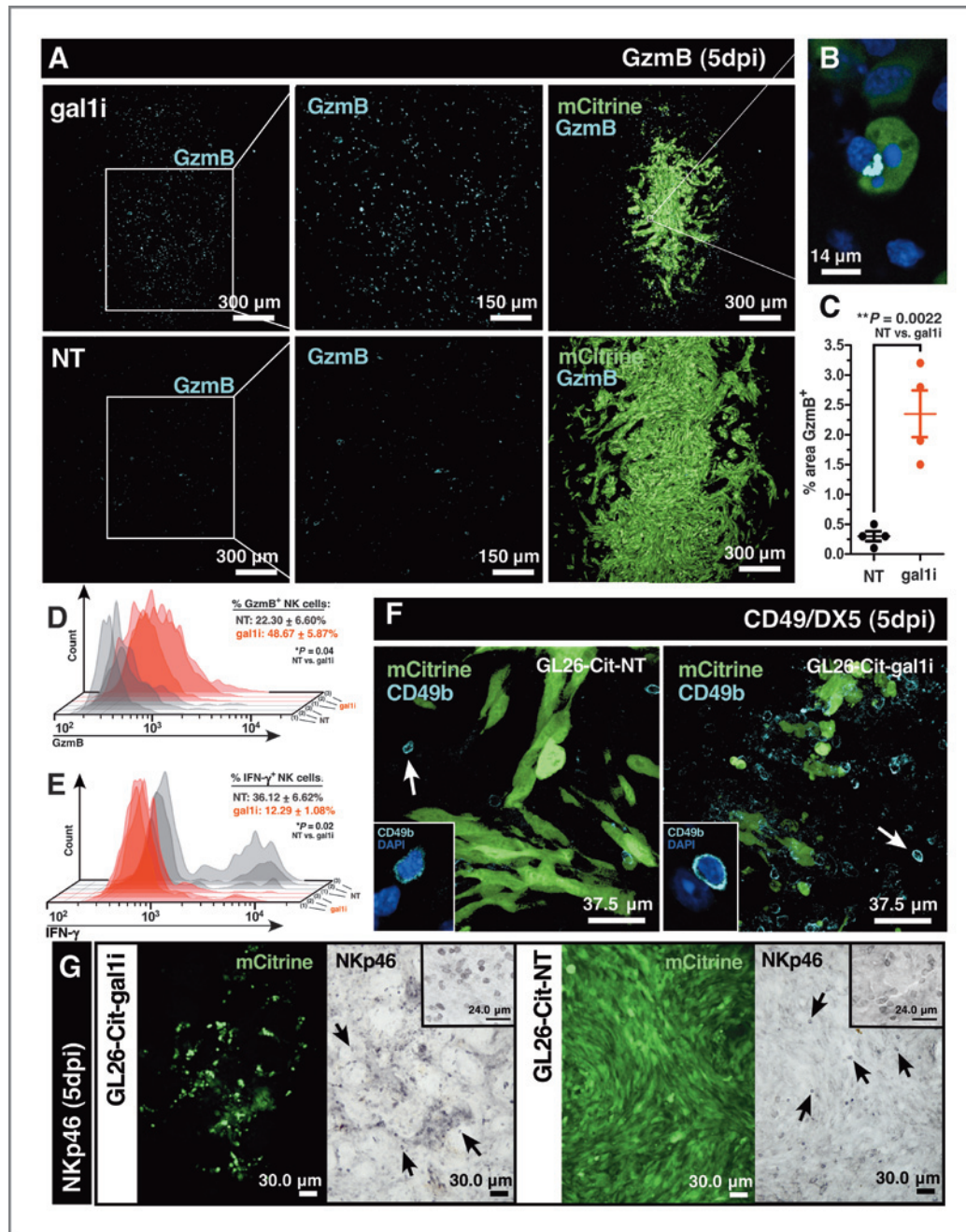


Figure 4. Gal-1-deficient gliomas are infiltrated with granzyme B⁺ NK cells. **A**, immunofluorescence with anti-granzyme B (GzmB) antibodies on RAG1^{-/-} mouse brain tissue sections bearing GL26-Cit-gal1i or GL26-Cit-NT gliomas 5 dpi. **B**, high-power image of an apoptotic GL26-Cit-gal1i cell associated with an accumulation of GzmB. **C**, percent area covered by GzmB immunolabeling from 20 distinct 10 \times brightfield micrographs using ImageJ analytical software. GL26-Cit-gal1i tumors contain significantly more immunopositive GzmB labeling (**, $P = 0.0022$; 2.35 \pm 0.39% gal1i vs. 0.30 \pm 0.08% GL26-Cit-NT; unpaired, two-tailed, Student *t* test). **D** and **E**, flow cytometric analysis of tumor-infiltrating NK cells from the cerebral hemisphere ipsilateral to the tumor implant in RAG1^{-/-} mice implanted with GL26-Cit-NT (gray histograms) or GL26-Cit-gal1i (red histograms) cells ($n = 6$; 3 mice/group) after 5 dpi. **D**, GL26-Cit-gal1i gliomas (red) contain significantly more GzmB⁺ NK cells (*, $P = 0.04$; 48.67 \pm 5.87% gal1i vs. 22.30 \pm 6.60% NT; unpaired, two-tailed, Student *t* test) compared with GL26-Cit-NT gliomas (gray). **E**, GL26-Cit-NT gliomas (gray) contain NK cells, which are significantly more IFN- γ ⁺ (*, $P = 0.02$; 36.12 \pm 6.62% NT vs. 12.29 \pm 1.08% gal1i; unpaired, two-tailed, Student *t* test) compared with NK cells in GL26-Cit-gal1i gliomas (red). **F**, immunofluorescence with anti-CD49b/DX5 antibodies on RAG1^{-/-} mouse brain tissue sections bearing GL26-Cit-NT or GL26-Cit-gal1i gliomas 5 dpi. White arrows, examples of CD49b/DX5⁺ NK cells shown at higher power in the insets. **G**, DAB/peroxidase immunohistochemistry with anti-NKp46 antibodies on RAG1^{-/-} mouse brain tissue sections bearing GL26-Cit-gal1i or GL26-Cit-NT gliomas 5 dpi. Black arrows, examples of NKp46⁺ NK cells. Insets provide alternative images at higher power.

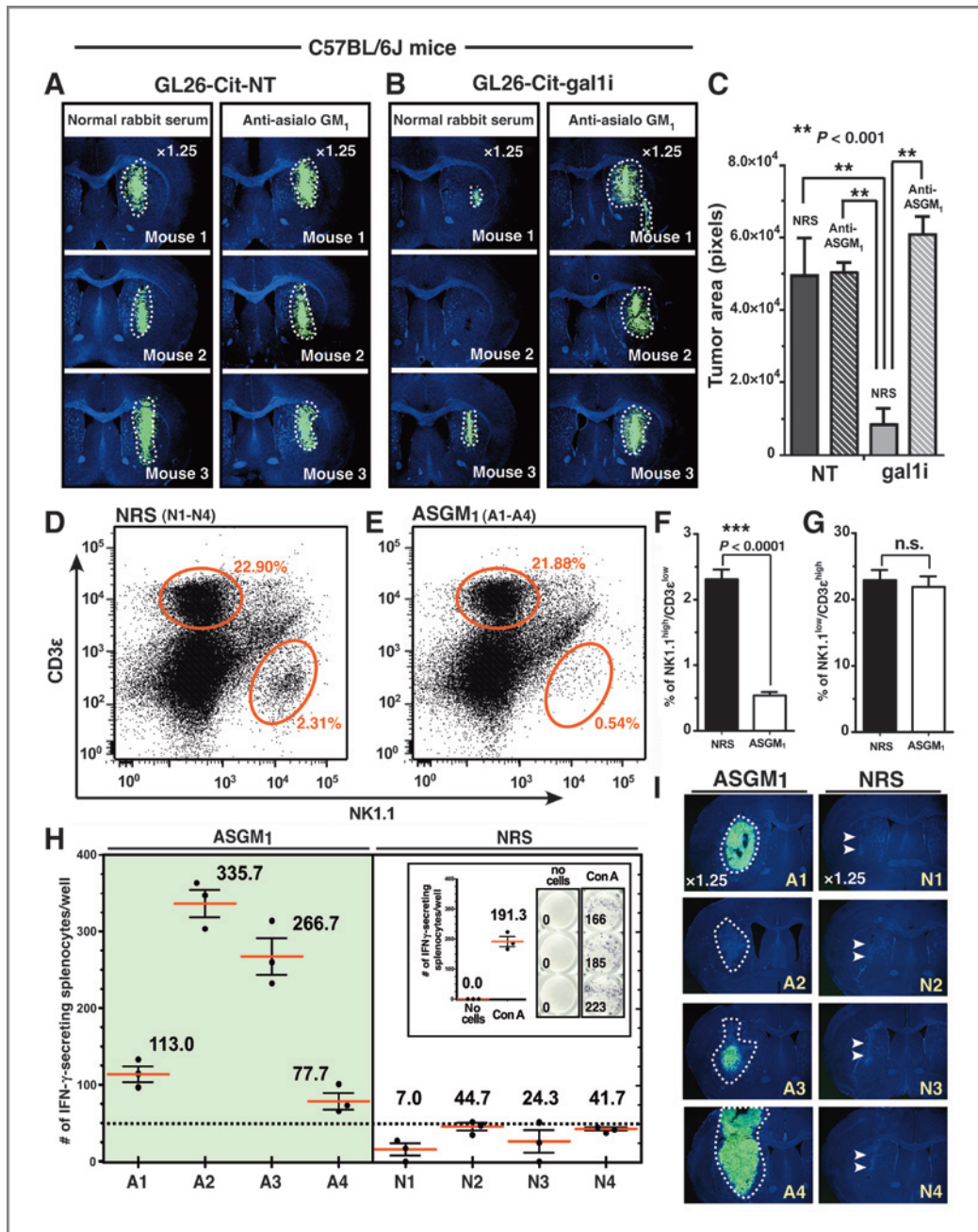


Figure 5. Gal-1-deficient glioma rejection occurs before the onset of antigen-specific adaptive immunity in fully immunocompetent mice. **A** and **B**, GL26-Cit-NT and GL26-Cit-gal1i cells within the C57BL/6J striatum treated with NRS or anti-asialo GM₁ after 5 dpi. **C**, quantification of tumor areas shown throughout **A** and **B** using ImageJ analytical software. GL26-Cit-gal1i tumors treated with NRS exhibited significantly smaller tumors compared with all other groups (**, $P < 0.001$ vs. gal1i treated with NRS; one-way ANOVA followed by Tukey posttest). **D** and **E**, flow cytometric plots of splenocytes immunolabeled with anti-NK1.1 and anti-CD3ε from C57BL/6J mice bearing GL26-Cit-gal1i gliomas treated with NRS (**D**) or ASGM₁ (**E**) for 16 dpi of ($n = 4$ mice/treatment group, merged data shown). Average percentages of NK1.1^{high}/CD3ε^{low} (i.e., NK cells) and NK1.1^{low}/CD3ε^{high} (i.e., T cells) in each treatment group are indicated by the respective red ovals. ASGM₁ treatment leads to a significant reduction in NK cells (***, $P < 0.0001$; 2.31 ± 0.15 NRS vs. 0.54 ± 0.05 ASGM₁; unpaired, two-tailed, Student *t* test) while leaving T cells unaffected (n.s., $P > 0.05$; 22.90 ± 1.51 NRS vs. 21.88 ± 1.58 ASGM₁; unpaired, two-tailed, Student *t* test; **F** and **G**, respectively). **H**, tumor antigen-induced mouse IFN γ ELISpot data. Splenocytes indicated in **D** and **E** were used. Splenocytes from mice treated with anti-asialo GM₁ produced high numbers of IFN γ spots, whereas only a nominal number of spots (<50) were produced by splenocytes from mice treated with NRS. The average number of IFN γ spots from three technical replicates are shown for each mouse (red bars). Positive (Con-A) and negative (no splenocyte) controls are shown (inset). **I**, GL26-Cit-gal1i brain tumors after 16 dpi corresponding to the animals indicated in **D**–**H**. Glioma growth (white dashed outlines) is seen in each ASGM₁-treated mice at various stages of tumor rejection. Conversely, only a scar at the site of the initial tumor implantation (double white arrowheads) is seen in each of the NRS-treated mice.

transcript in mouse GL26 glioma. We became interested in testing the role of this gene in brain tumor growth and invasion because tumor-derived gal-1 is associated with increasing malignancy and poor patient prognosis in clinical glioma (Supplementary Fig. S2; refs. 13 and 14).

We began by determining whether gal-1 was also expressed by a fluorescently modified version of GL26 referred to as GL26-Cit (24). Western blot analysis and immunohistochemistry confirmed the expression of gal-1 by GL26-Cit cells (Fig. 1A and B). We validated five commercially available gal-1–specific shRNA hairpins from the RNAi consortium (TRC) and chose the one that exhibited the highest degree of gal-1 knockdown for stable incorporation into GL26-Cit cells by lentiviral-mediated gene transfer. Resultant gal-1–deficient cells were referred to as GL26-Cit-gal1i. These cells exhibited a 60% reduction in gal-1 protein expression relative to control GL26-Cit cells transduced with lentiviruses expressing a nontargeting shRNA (GL26-Cit-NT) or an empty shRNA expression vector (GL26-Cit-EV; Fig. 1A and C and Supplementary Fig. S3A). Two independent transductions of either gal-1–specific-, or control-, shRNA hairpins were performed (Supplementary Fig. S3).

To characterize the growth and behavior of GL26-Cit-gal1i *in vitro*, we first performed ELISA analysis for secreted gal-1, which revealed that GL26-Cit-gal1i cells release half as much gal-1 into cell culture media compared with equivalent numbers of GL26-Cit-NT (Fig. 1D). We also determined the average cell doubling time of GL26-Cit-gal1i cells compared with GL26-Cit-NT over a 96-hour growth period starting from an initial seeding density of 4.8×10^2 cells per cm^2 . Both cell lines displayed cell doubling times of approximately 16 hours (Fig. 1E) with no significant differences in the rate of spontaneous apoptosis (Supplementary Fig. S4). *In vitro* scratch assays were performed to evaluate the migration speed of GL26-Cit-gal1i cells compared with GL26-Cit-NT. GL26-Cit-gal1i cells exhibited a nearly 25% increase in migration distance compared with GL26-Cit-NT when cultured on fibronectin, a binding partner for heterotypic gal-1 interaction (Fig. 1F; ref. 25).

To assess GL26-Cit-gal1i growth *in vivo*, we implanted 3×10^4 cells into the striatum of $\text{RAG1}^{-/-}$ mice (26) and compared their invasion characteristics to control GL26-Cit, GL26-Cit-EV, and GL26-Cit-NT cells after 48 hours. We used $\text{RAG1}^{-/-}$ mice, which do not produce mature T and B cells, to avoid antigen-specific adaptive immunity against mCitrine fluorescent protein so not to obscure our analysis of tumor invasion. Tumor morphology was analyzed by fluorescence confocal microscopy of tumor-derived mCitrine. Control GL26-Cit cell lines expressing normal gal-1 levels displayed a diffuse growth pattern indicative of perivascular tumor invasion, whereas GL26-Cit-gal1i cells remained confined to the site of initial tumor implantation (Fig. 1G). This effect was quantified by comparing the morphologies of GL26-Cit-gal1i gliomas with controls using ImageJ analytical software (Supplementary Fig. S5).

Gal-1–deficient glioma cells undergo early caspase-3–dependent cell death upon implantation into the $\text{RAG1}^{-/-}$ mouse brain

Encouraged by our observation that GL26-Cit-gal1i glioma cells fail to invade the mouse brain, we wished to test whether

gal-1 suppression would improve the median survival of mice bearing GL26-Cit glioma. Kaplan–Meier survival analysis was carried out on $\text{RAG1}^{-/-}$ mice implanted with 3×10^4 GL26-Cit-gal1i, GL26-Cit, or GL26-Cit-NT glioma cells to compare their survival rates (Fig. 2A). All mice in the GL26-Cit and GL26-Cit-NT groups became moribund by day 20 posttumor implantation, yet each mouse implanted with GL26-Cit-gal1i cells survived 100 days posttumor implantation (dpi). Mice implanted with GL26-Cit-gal1i cells were then electively euthanized to assess tumor burden. Although GL26-Cit and GL26-Cit-NT cells formed tumors comprising most of the ipsilateral striatum after 20 days *in vivo*, only nonviable remnants of mCitrine were found in the brain of mice implanted with GL26-Cit-gal1i cells after the 100th day *in vivo* (Fig. 2B).

To characterize the fate of intracranially implanted GL26-Cit-gal1i cells, we analyzed tumors corresponding to seven time-points over a 9-day growth period ($n = 21$; 3 mice/time-point). Fluorescence immunohistochemistry for cleaved caspase-3, a major downstream effector caspase-mediated apoptotic cell death (27), revealed large numbers of GL26-Cit-gal1i cells undergoing apoptotic cell death, especially at the invasive tumor margin, within 3 days of tumor implantation (Fig. 2C). Later tumors exhibited exacerbated lysis culminating in

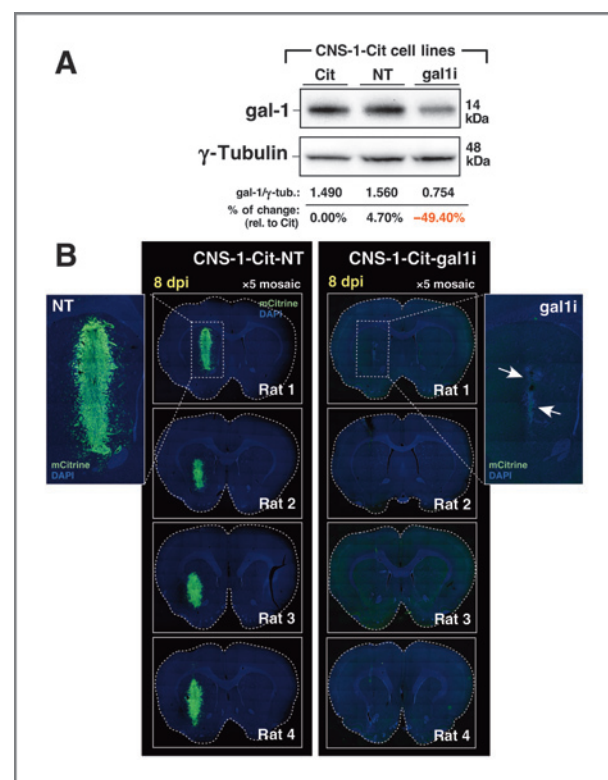


Figure 6. Gal-1–deficient rat CNS-1-Cit glioma cells fail to form intracranial tumors in syngeneic Lewis rats. **A**, Western blot analysis for gal-1 in rat CNS-1-Cit glioma. Cit, CNS-1-Cit; NT, CNS-1-Cit-NT; gal1i, CNS-1-Cit-gal1i. **B**, dual-channel epifluorescence 5 \times mosaic microscopy of Lewis rat brain sections bearing CNS-1-Cit-NT or CNS-1-Cit-gal1i 8 dpi. Dashed white boxes in the top two micrographs are shown at higher magnification for clarity. White arrows in the GL26-Cit-gal1i example point to the nonviable tumor remnant.

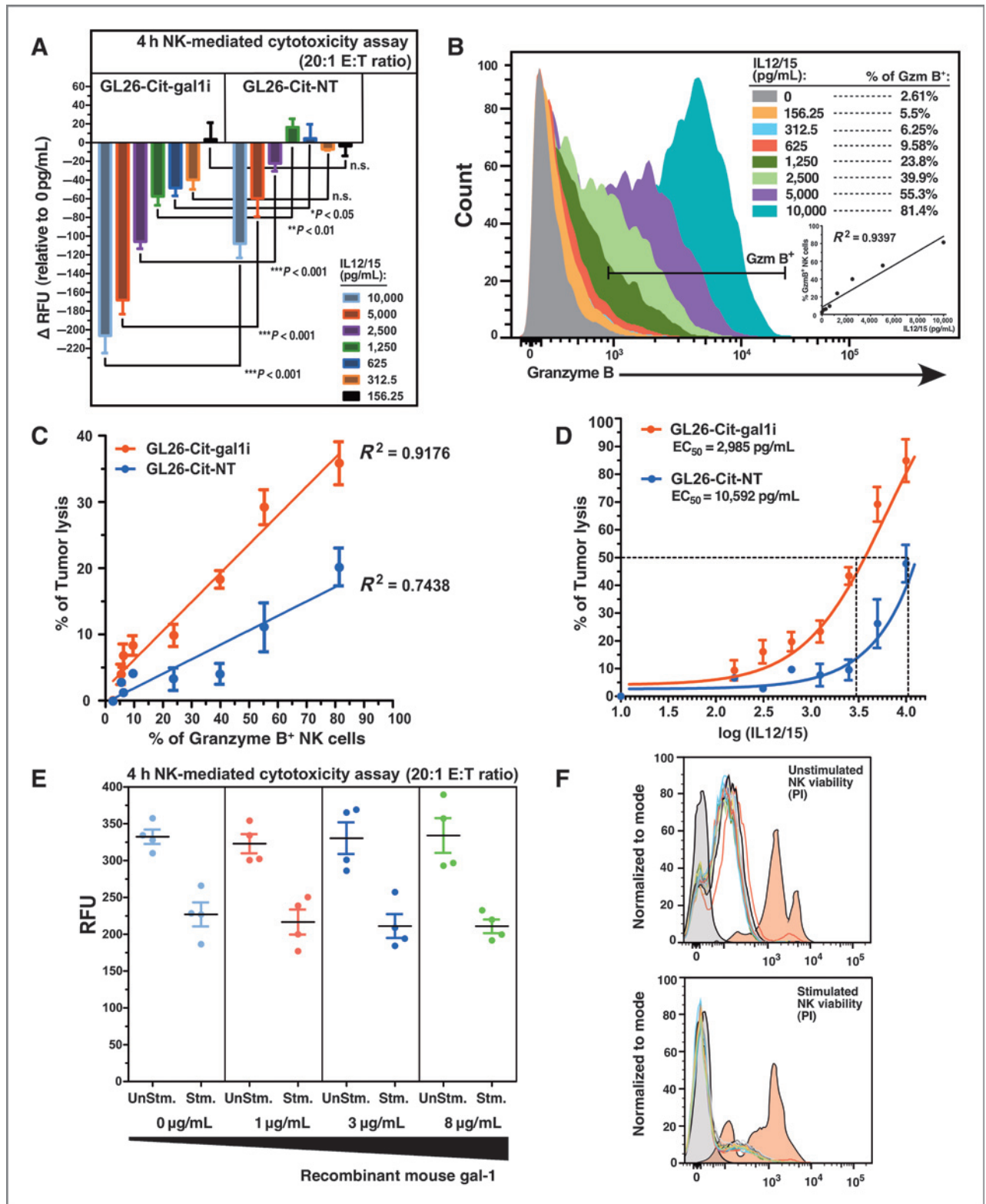


Figure 7. Gal-1-deficient glioma cells are sensitized to NK-mediated tumor lysis. **A**, change in fluorescence intensity signals (Δ RFU) from GL26-Cit-gal1i or GL26-Cit-NT cells after 4-hour cocubation with splenic-derived RAG1^{-/-} NK cells stimulated overnight with the indicated concentrations of IL12/15. GL26-Cit-gal1i cells lysed more readily in response to NK cells stimulated with all IL12/15 concentrations above 312.5 pg/mL (*, $P < 0.05$ vs. GL26-Cit-NT; two-way ANOVA). **B**, flow cytometric analysis for GzmB⁺ NK cells after overnight culture in increasing concentrations of IL12/15. Linear regression analysis comparing IL12/15 concentration with % GzmB⁺ NK cells ($R^2 = 0.9397$). (Continued on the following page.)

complete tumor lysis after 9 days *in vivo* (Fig. 2D). Interestingly, antibodies against cleaved caspases 8 and 9, initiator caspases of the extrinsic and intrinsic caspase cascades, respectively, failed to detect activated upstream caspases (data not shown), suggesting that pro-caspase-3 was being cleaved directly.

We considered that the innate immune system might play a role in the regression of GL26-Cit-gal1 glioma in the RAG1^{-/-} model. To test this hypothesis, we implanted GL26-Cit-gal1 cells into the striatum of NOD-*scid* IL2Rg^{null} (i.e., NSG) mice, a mouse strain lacking both innate and adaptive immunity (28), for comparison with GL26-Cit-NT cells ($n = 6$; 3 mice/group). We reasoned that if the RAG1^{-/-} innate immune system was responsible for GL26-Cit-gal1 regression, then GL26-Cit-gal1 tumor growth should be restored on implantation into NSG mice. Our hypothesis was substantiated, as 3×10^4 GL26-Cit-gal1 or GL26-Cit-NT cells both formed lethal brain tumors in NSG mice after 16 days *in vivo* (Fig. 2E). The combined results of GL26-Cit-gal1 rejection in RAG1^{-/-} mice, and the restoration of lethal tumor growth in NSG mice, strongly implicated the innate immune response in the acute rejection of intracranial GL26-Cit-gal1 glioma.

NK cells mediate the acute rejection of intracranial gal-1-deficient glioma

NK cells lyse tumor target cells through the release of granzyme B (GzmB), an enzyme that directly cleaves pro-caspase-3 (29–31). Because our data had shown that GL26-Cit-gal1 tumors were positive for cleaved caspase-3, yet negative for activated upstream initiator caspases-8 and -9, we questioned whether NK cells are responsible for GL26-Cit-gal1 rejection in RAG1^{-/-} mice. We therefore treated RAG1^{-/-} mice bearing GL26-Cit-gal1 glioma with anti-asialo GM₁, an antiserum validated by ourselves (Supplementary Fig. S6A and S6B), and others (32), to deplete NK cells in mice, or with NRS as a negative control. Mice were euthanized 16 dpi and their brains were imaged using epifluorescence microscopy. Treatment with anti-asialo GM₁ caused the formation of large intracranial GL26-Cit-gal1 tumors, whereas treatment with NRS control failed to do so (Fig. 3A).

We tested whether the growth of GL26-Cit-gal1 glioma permitted by anti-asialo GM₁ was mediated by off-target depletion of basophils as previously described (33). Cohorts of RAG1^{-/-} mice was treated with anti-CD200R3 (clone: Ba103), a monoclonal antibody validated for *in vivo* depletion of basophils (34) or rat IgG2b isotype control antibodies at an equivalent dose, route, and schedule. Both anti-CD200R3 and rat IgG2b isotype control antibodies failed to permit intracranial GL26-Cit-gal1 tumor growth in RAG1^{-/-} mice after a 10-day growth period (Supplementary Fig. S6C), indicating that basophils are not responsible for gal-1-deficient glioma rejection in RAG1^{-/-} mice.

We confirmed our results with anti-asialo GM₁ using purified functional-grade anti-NK1.1 (clone: PK136; ref. 35), an alternative monoclonal antibody validated for *in vivo* NK depletion in mice on a B6 background. RAG1^{-/-} mice treated with anti-NK1.1 also formed large GL26-Cit-gal1 tumors of equivalent size to those obtained with anti-asialo GM₁ (Fig. 3B).

Gal-1-deficient gliomas are more heavily infiltrated with granzyme B⁺ NK cells

We next sought to evaluate the presence of glioma-infiltrating NK cells. We implanted 3×10^4 GL26-Cit-gal1 or GL26-Cit-NT cells into the striatum of RAG1^{-/-} mice and allowed for 5 days of tumor growth ($n = 6$; 3 mice/group). Mouse brains were harvested, sectioned, and immunolabeled with GzmB-specific antibodies. Quantitative analysis revealed that GL26-Cit-gal1 tumors contain nearly 8 times more GzmB compared with GL26-Cit-NT (Fig. 4A–C).

Because RAG1^{-/-} mice do not produce mature T lymphocytes, the GzmB signal seen in GL26-Cit-gal1 tumors was reasoned to be NK specific. To confirm this, we performed multicolor flow cytometric analysis on glioma-infiltrating NK cells using antibodies against CD45, NK1.1, CD3ε, GzmB, and IFNγ after 5 days of *in vivo* growth in the RAG1^{-/-} mouse brain. GL26-Cit-gal1 tumors contained significantly higher percentages of GzmB⁺ NK cells compared with GL26-Cit-NT ($48.67 \pm 5.87\%$ gal1 vs. $22.30 \pm 6.60\%$ NT; Fig. 4D), whereas GL26-Cit-NT gliomas contained significantly higher percentages of IFNγ⁺ NK cells ($36.12 \pm 6.62\%$ NT vs. $12.29 \pm 1.08\%$ gal1; Fig. 4E). Further confirmation of tumor-infiltrating NK cells was obtained through immunohistochemistry with alternative NK-specific antibodies CD49b/DX5 (Fig. 4F) and NKP46 (Fig. 4G), which indicate that NK cells are capable of infiltrating both NT and gal1 gliomas.

NK cells eradicate gal-1-deficient glioma before the initiation of an adaptive immune response

We next investigated the effect of NK cells on the rejection of gal-1-deficient glioma in fully immunocompetent hosts. We implanted 3×10^4 GL26-Cit-gal1 or GL26-Cit-NT cells into the striatum of wild-type C57BL/6J mice and treated these mice with anti-asialo GM₁ or control serum for 5 days before sacrifice ($n = 12$; 3 mice/group/treatment). Restriction of our analysis to the first 5 dpi allowed us to isolate the innate immune response, as antigen-specific adaptive immunity does not peak until ~10 to 14 dpi (36–40). Mice implanted with GL26-Cit-NT cells formed equivalently sized tumors after 5 days of growth regardless of treatment with anti-asialo GM₁ or control serum (Fig. 5A). However, mice implanted with GL26-Cit-gal1 only formed tumors similar in size to GL26-Cit-NT when treated with NK-depleting anti-asialo GM₁ (Fig. 5B). We

(Continued.) C, linear regression analysis comparing the percentage of GzmB⁺ NK cells and % tumor cells lysis in GL26-Cit-gal1 cells and GL26-Cit-NT cells. D, sigmoidal dose-response curve fitting of log-transformed IL12/15 concentration versus the percentage of tumor lysis. Calculated EC₅₀s for NK-mediated cytotoxicity are shown. E, 4-hour NK-mediated cytotoxicity assay using splenic-derived NK cells from C57BL/6J mice targeting GL26-Cit-gal1 cells at a 20:1 E:T ratio. The presence of increasing concentrations of recombinant mouse gal-1 protein fails to inhibit NK-mediated tumor lysis in response to stimulation with 10,000 pg/mL IL12/15 ($n = 3$ wells/group). F, propidium iodide NK viability assay on stimulated or unstimulated NK cells in the presence of recombinant mouse gal-1 protein. Increasing concentrations of recombinant gal-1 protein fails to induce apoptosis in both NK populations. Unstained negative control (gray histograms) and staurosporine-treated positive control (red histograms) are shown.

quantified this effect by calculating the average tumor area in each treatment group using ImageJ analytical software (Fig. 5C). GL26-Cit-galli tumors treated with control serum were significantly smaller than those in the 3 other treatment groups. This result shows that the NK cells from fully immunocompetent hosts are capable of efficiently eradicating gal-1-deficient glioma.

We then asked whether the innate immune system could effectively eliminate GL26-Cit-galli glioma before the initiation of an antigen-specific adaptive immune response. To address this, we implanted 3×10^4 GL26-Cit-galli cells into the striatum of wild-type C57BL/6J mice, and treated mice with either anti-asialo GM₁ or control serum for 16 days before sacrifice to provide enough time for the onset of antigen-specific adaptive immunity. The brain and spleen of each mouse were freshly harvested at the time of sacrifice and a fraction of total splenocytes from each mouse was immunolabeled with anti-NK1.1 and anti-CD3e antibodies to assess NK cell depletion by flow cytometric analysis. Mice treated with anti-asialo GM₁ exhibited a >4-fold reduction in the average percentage of splenic-derived NK cells without altering the average percentage of T cells (Fig. 5D–G).

The remaining splenocytes were used in antigen-induced ELISpot analysis to evaluate the number of splenocytes secreting IFN γ in response to GL26-Cit-galli lysate after 48 hours *in vitro*. This assay served as a surrogate indicator of the degree of adaptive immune activation elicited against GL26-Cit-galli brain tumors over the 16-day growth period. ELISpot results revealed that more splenocytes from mice treated with anti-asialo GM₁ secreted IFN γ in response to addition of GL26-Cit-galli lysate compared with those treated with NRS (Fig. 5H). This suggested that GL26-Cit-galli tumors were present in the brain long enough to be recognized by the adaptive immune response in mice depleted of NK cells. However, the paucity of splenocytes secreting IFN γ in response to GL26-Cit-galli lysate from mice treated with control serum indicated that NK cells eradicate GL26-Cit-galli tumors before recognition by antigen-specific antitumor immunity. Analysis of corresponding brain tumor size confirmed this notion by showing that gliomas were present in the brains of mice treated with anti-asialo GM₁, whereas no tumors were seen in the brains of mice treated with NRS (Fig. 5I). We observed a strong inverse Pearson's product-moment correlation coefficient ($r = -0.91$) between the average number of IFN γ spots from our ELISpot analysis and the corresponding tumor size in mice treated with anti-asialo GM₁. We conclude that reductions in brain tumor burden in mice lacking NK cells correlates with the magnitude of antigen-specific adaptive immunity. Immunohistochemistry with anti-CD3e antibodies revealed that only the mice treated with anti-asialo GM₁ contained brain-infiltrating T cells (Supplementary Fig. S7).

Gal-1-deficient rat CNS-1-Cit glioma cells fail to grow intracranially

We have asked whether gal-1-deficient glioma of other species fail to grow intracranially. For this, we validated gal-1 expression in fluorescently modified rat CNS-1 glioma cells also expressing mCitrine fluorescent protein, referred to as

CNS-1-Cit. Gal-1 expression was silenced through stable incorporation of gal-1-specific shRNA by lentiviral-mediated gene transfer to generate CNS-1-Cit-galli. CNS-1-Cit-galli cells exhibited a 50% reduction in gal-1 protein expression relative to control CNS-1-Cit cells infected with lentiviruses expressing a nontargeting shRNA referred to as CNS-1-Cit-NT (Fig. 6A). We implanted 3×10^4 CNS-1-Cit-galli or CNS-1-Cit-NT cells into the striatum of syngeneic Lewis rats and electively euthanized after 8 dpi to preclude the onset of an adaptive antitumor immune response. Although CNS-1-Cit-NT cells formed viable tumors in each rat brain after the 8-day growth period, CNS-1-Cit-galli tumors were completely rejected, leaving remnants of mCitrine at the site of initial tumor implantation (Fig. 6B). We conclude that gal-1 suppression sensitizes glioma of diverse species to innate immune attack.

Gal-1-deficient glioma cells are sensitized to NK-mediated cytotoxicity *in vitro*

We next examined the efficiency of NK-mediated gal-1-deficient tumor lysis *in vitro*. Splenic-derived NK cells were isolated from tumor-naïve RAG1^{-/-} mice by FACS and determined to be >95% pure (Supplementary Fig. S8). NK cells were prestimulated overnight in round-bottom wells with 8 concentrations of interleukin 12 (IL12) and interleukin 15 (IL15) from 0 to 10,000 pg/mL of each cytokine. Stimulated NK cells were added to both GL26-Cit-galli and GL26-Cit-NT glioma cells at an effector-to-target (E:T) ratio of 20:1 and incubated for 4 hours at 37°C/5% CO₂. Although unstimulated NK cells failed to induce lysis in either glioma cell line, GL26-Cit-galli cells lysed more readily after the 4-hour co-incubation with NK cells stimulated with IL12/15 concentrations above 312.5 pg/mL (Fig. 7A). Linear regression analysis comparing IL12/15 concentration with the resultant percentage of GzmB⁺ NK cells after overnight stimulation revealed an R^2 value of 0.94 ($R^2 = 0.94$), demonstrating that IL12/15 stimulation strongly correlates with GzmB production by splenic-derived NK cells (Fig. 7B).

Linear regression analysis also revealed a positive correlation between the percentage of GzmB⁺ NK cells and the percentage of tumor lysis in the GL26-Cit-galli group ($R^2 = 0.92$), which were less correlated in the GL26-Cit-NT group ($R^2 = 0.74$; Fig. 7C). We interpret this result as an indicator of NK cytotoxic potential; how other NK proteins relate to tumor NK cytotoxicity remains to be determined (41, 42). The reduced correlation between GzmB expression and tumor lysis in the GL26-Cit-NT group suggested that gal-1 expression imparts glioma cells with intrinsic resistance to NK-mediated tumor lysis. A sigmoidal dose-response fitting of log-transformed IL12/15 concentration versus percentage tumor lysis revealed corresponding EC₅₀ values for IL12/15 stimulation (i.e., amount of IL12/15 required to elicit 50% tumor cell lysis) of 2,985 and 10,592 pg/mL for GL26-Cit-galli and GL26-Cit-NT cells, respectively. This result demonstrates that GL26-Cit-galli cells are 3.55-fold more sensitive to NK-mediated cytotoxicity compared with GL26-Cit-NT *in vitro* (Fig. 7D).

To test whether gal-1 directly inhibits NK-cell function or viability, we added recombinant mouse gal-1 protein at increasing concentrations to NK/GL26-Cit-galli *in vitro* cocultures. Unstimulated splenic-derived NK cells failed to induce tumor

cell lysis, whereas those stimulated with 10,000 pg/mL IL12/15 induced tumor cell death after 4-hour cocultivation. However, application of increasing levels of recombinant gal-1 protein failed to inhibit NK-mediated cytotoxicity (Fig. 7E) or induce apoptosis in either unstimulated or stimulated NK cells (Fig. 7F).

Discussion

We have identified glioma-derived galectin-1 as a potent suppressor of antitumor NK immune surveillance. Five *in vivo* experimental results support this conclusion: (i) gal-1-deficient glioma cells fail to form lethal brain tumors upon orthotopic implantation into the RAG1^{-/-} mouse brain; (ii) lethal gal-1-deficient glioma growth is restored upon implantation into the brains of NOD-*scid* IL2Rg^{null} mice; (iii) immunodepletion of NK cells with anti-asialo GM₁ anti-serum, or anti-NK1.1 monoclonal antibodies permit the formation of lethal gal-1-deficient gliomas in RAG1^{-/-} mice; (iv) gal-1-deficient gliomas in RAG1^{-/-} mice contain more GzmB⁺ NK cells; and (v) NK cells eradicate gal-1-deficient gliomas in fully immunocompetent C57BL/6J mice before the initiation of antitumor T-cell responses.

Flow cytometric and immunohistochemical data on tumor-infiltrating NK cells demonstrate the accumulation of GzmB⁺ NK cells specifically within gal-1-deficient gliomas soon after implantation. However, gliomas expressing normal levels of gal-1 are infiltrated with NK cells that predominantly produce IFN γ instead of GzmB.

Experiments in fully immunocompetent C57BL/6J mice demonstrated that the innate immune system rejects gal-1-deficient glioma without the support of antigen-specific antitumor adaptive immunity. This is shown by the absence of growing brain tumors and antitumor T-cell responses in mice treated with control antiserum. As expected, in the absence of NK cells, gal-1-deficient gliomas are targets of tumor-specific cytotoxic T cells, albeit later in tumor progression. This is evidenced by the negative correlation between the levels of antigen-specific T-cell responses and brain tumor size in immunocompetent mice depleted of NK cells.

Glioma cells evade cytotoxic T-cell recognition and lysis by downregulating MHC class-I proteins (43, 44). However, this process increases their sensitivity to NK-mediated attack, as cells with reduced expression of MHC class-I proteins are targets of NK immune surveillance (43). Upregulation of gal-1 expression may therefore provide an advantage for glioma cells

to concurrently curb both arms of the antitumor immune response by counteracting the increased sensitivity to NK immune surveillance associated with MHC-1 downregulation.

Our results introduce a paradigm shift in the current understanding of anti-glioma immune-mediated control by showing for the first time that NK cells, even in the absence of adaptive immunity, eradicate intracranial glioma in the context of reduced tumor-derived gal-1. We predict that gal-1 suppression; either alone or in combination with other immunotherapeutic strategies (i.e., dendritic cell vaccination; refs. 45, 46) and/or gene therapy (47–50) will provide dramatic clinical improvements in patients suffering from malignant brain tumors.

Disclosure of Potential Conflicts of Interest

No potential conflicts of interest were disclosed.

Authors' Contributions

Conception and design: G.J. Baker, M.G. Castro, P.R. Lowenstein

Development of methodology: G.J. Baker, P. Chockley, V.N. Yadav, P.R. Lowenstein

Acquisition of data (provided animals, acquired and managed patients, provided facilities, etc.): G.J. Baker, P. Chockley, V.N. Yadav, R. Doherty, M. Ritt, S. Sivaramakrishnan, P.R. Lowenstein

Analysis and interpretation of data (e.g., statistical analysis, biostatistics, computational analysis): G.J. Baker, P. Chockley, V.N. Yadav, R. Doherty, M. Ritt, S. Sivaramakrishnan, M.G. Castro, P.R. Lowenstein

Writing, review, and/or revision of the manuscript: G.J. Baker, S. Sivaramakrishnan, M.G. Castro, P.R. Lowenstein

Administrative, technical, or material support (i.e., reporting or organizing data, constructing databases): G.J. Baker, P.R. Lowenstein

Study supervision: G.J. Baker, M.G. Castro, P.R. Lowenstein

Other (overall funding, design, implementation, analysis of this project): M. Castro, P.R. Lowenstein

Acknowledgments

We gratefully acknowledge support for our work received from Philip Jenkins, and the Department of Neurosurgery, University of Michigan School of Medicine. The authors thank Dr. Karin Muraszko for her academic leadership, Molly Dahlgren, D. Tomford, and S. Napolitan for their superb administrative support, and Dr. Roger Tsien (UCSD) for kindly donating the pRSET-B-mCitrine plasmid.

Grant Support

This work was supported by NIH/National Institute of Neurological Disorders & Stroke (NIH/NINDS) grants 1R01-NS 054193, 1R01-NS 061107, and 1R01-NS082311 (P.R. Lowenstein); and grants 1U01-NS052465, 1R01-NS 057711, and 1R01-NS074387 (M.G. Castro).

The costs of publication of this article were defrayed in part by the payment of page charges. This article must therefore be hereby marked *advertisement* in accordance with 18 U.S.C. Section 1734 solely to indicate this fact.

Received April 23, 2014; revised June 2, 2014; accepted July 1, 2014; published OnlineFirst July 18, 2014.

References

- Vivier E, Raulet DH, Moretta A, Caligiuri MA, Zitvogel L, Lanier LL, et al. Innate or adaptive immunity? The example of natural killer cells. *Science* 2011;331:44–9.
- Vivier E, Tomasello E, Baratin M, Walzer T, Ugolini S. Functions of natural killer cells. *Nat Immunol* 2008;9:503–10.
- Bryceson YT, March ME, Ljunggren HG, Long EO. Activation, coactivation, and costimulation of resting human natural killer cells. *Immunol Rev* 2006;214:73–91.
- Smyth MJ, Hayakawa Y, Takeda K, Yagita H. New aspects of natural killer-cell surveillance and therapy of cancer. *Nat Rev Cancer* 2002;2:850–61.
- Wu H, Chen P, Liao R, Li YW, Yi Y, Wang JX, et al. Overexpression of galectin-1 is associated with poor prognosis in human hepatocellular carcinoma following resection. *J Gastroenterol Hepatol* 2012;27:1312–9.
- Kim HJ, Jeon HK, Cho YJ, Park YA, Choi JJ, Do IG, et al. High galectin-1 expression correlates with poor prognosis and is involved in epithelial ovarian cancer proliferation and invasion. *Eur J Cancer* 2012;48:1914–21.
- van den Brule FA, Waltregny D, Castronovo V. Increased expression of galectin-1 in carcinoma-associated stroma predicts poor outcome in prostate carcinoma patients. *J Pathol* 2001;193:80–7.

8. Kohrenhagen N, Volker HU, Kapp M, Dietl J, Kammerer U. Increased expression of galectin-1 during the progression of cervical neoplasia. *Int J Gynecol Cancer* 2006;16:2018–22.
9. Sanjuan X, Fernandez PL, Castells A, Castronovo V, van den Brule F, Liu FT, et al. Differential expression of galectin 3 and galectin 1 in colorectal cancer progression. *Gastroenterology* 1997;113:1906–15.
10. Berberat PO, Friess H, Wang L, Zhu Z, Bley T, Frigeri L, et al. Comparative analysis of galectins in primary tumors and tumor metastasis in human pancreatic cancer. *J Histochem Cytochem* 2001;49:539–49.
11. Chiariotti L, Berlingieri MT, Battaglia C, Benvenuto G, Martelli ML, Salvatore P, et al. Expression of galectin-1 in normal human thyroid gland and in differentiated and poorly differentiated thyroid tumors. *Int J Cancer* 1995;64:171–5.
12. van den Brule FA, Buicu C, Berchuck A, Bast RC, Deprez M, Liu FT, et al. Expression of the 67-kD laminin receptor, galectin-1, and galectin-3 in advanced human uterine adenocarcinoma. *Hum Pathol* 1996;27:1185–91.
13. Camby I, Belot N, Rorive S, Lefranc F, Maurage CA, Lahm H, et al. Galectins are differentially expressed in supratentorial pilocytic astrocytomas, astrocytomas, anaplastic astrocytomas and glioblastomas, and significantly modulate tumor astrocyte migration. *Brain Pathol* 2001;11:12–26.
14. Rorive S, Belot N, Decaestecker C, Lefranc F, Gordower L, Micic S, et al. Galectin-1 is highly expressed in human gliomas with relevance for modulation of invasion of tumor astrocytes into the brain parenchyma. *Glia* 2001;33:241–55.
15. Perillo NL, Pace KE, Seilhamer JJ, Baum LG. Apoptosis of T cells mediated by galectin-1. *Nature* 1995;378:736–9.
16. Rubinstein N, Alvarez M, Zwirner NW, Toscano MA, Ilarregui JM, Bravo A, et al. Targeted inhibition of galectin-1 gene expression in tumor cells results in heightened T cell-mediated rejection; a potential mechanism of tumor-immune privilege. *Cancer Cell* 2004;5:241–51.
17. Gieseke F, Bohringer J, Bussolari R, Dominici M, Handgretinger R, Muller I. Human multipotent mesenchymal stromal cells use galectin-1 to inhibit immune effector cells. *Blood* 2010;116:3770–9.
18. Banh A, Zhang J, Cao H, Bouley DM, Kwok S, Kong C, et al. Tumor galectin-1 mediates tumor growth and metastasis through regulation of T-cell apoptosis. *Cancer Res* 2011;71:4423–31.
19. Soldati R, Berger E, Zenclussen AC, Jorch G, Lode HN, Salatino M, et al. Neuroblastoma triggers an immunoevasive program involving galectin-1-dependent modulation of T cell and dendritic cell compartments. *Int J Cancer* 2012;131:1131–41.
20. Kovacs-Solyom F, Blasko A, Fajka-Boja R, Katona RL, Vegh L, Novak J, et al. Mechanism of tumor cell-induced T-cell apoptosis mediated by galectin-1. *Immunol Lett* 2010;127:108–18.
21. Cedeno-Laurent F, Watanabe R, Teague JE, Kupper TS, Clark RA, Dimitroff CJ. Galectin-1 inhibits the viability, proliferation, and Th1 cytokine production of nonmalignant T cells in patients with leukemic cutaneous T-cell lymphoma. *Blood* 2012;119:3534–8.
22. Puntel M, Kroeger KM, Sanderson NS, Thomas CE, Castro MG, Lowenstein PR. Gene transfer into rat brain using adenoviral vectors. *Curr Protoc Neurosci* 2010;4:24.
23. Curtin JF, Liu N, Candolfi M, Xiong W, Assi H, Yagiz K, et al. HMGB1 mediates endogenous TLR2 activation and brain tumor regression. *PLoS Med* 2009;6:e10.
24. Baker GJ, Yadav VN, Motsch S, Koschmann C, Calinescu AA, Mineharu Y, et al. Mechanisms of glioma formation: iterative perivascular glioma growth and invasion leads to tumor progression, VEGF-independent vascularization, and resistance to antiangiogenic therapy. *Neoplasia* 2014;16:543–61.
25. Ozeki Y, Matsui T, Yamamoto Y, Funahashi M, Hamako J, Titani K. Tissue fibronectin is an endogenous ligand for galectin-1. *Glycobiology* 1995;5:255–61.
26. Mombaerts P, Iacomini J, Johnson RS, Herrup K, Tonegawa S, Papaioannou VE. RAG-1-deficient mice have no mature B and T lymphocytes. *Cell* 1992;68:869–77.
27. Tewari M, Quan LT, O'Rourke K, Desnoyers S, Zeng Z, Beidler DR, et al. Yama/CPBP32 beta, a mammalian homolog of CED-3, is a CrmA-inhibitable protease that cleaves the death substrate poly(ADP-ribose) polymerase. *Cell* 1995;81:801–9.
28. Shultz LD, Lyons BL, Burzenski LM, Gott B, Chen X, Chaleff S, et al. Human lymphoid and myeloid cell development in NOD/LtSz-scid IL2R gamma null mice engrafted with mobilized human hemopoietic stem cells. *J Immunol* 2005;174:6477–89.
29. Barry M, Heibei JA, Pinkoski MJ, Lee SF, Moyer RW, Green DR, et al. Granzyme B short-circuits the need for caspase 8 activity during granule-mediated cytotoxic T-lymphocyte killing by directly cleaving Bid. *Mol Cell Biol* 2000;20:3781–94.
30. Goping IS, Barry M, Liston P, Sawchuk T, Constantinescu G, Michalak KM, et al. Granzyme B-induced apoptosis requires both direct caspase activation and relief of caspase inhibition. *Immunity* 2003;18:355–65.
31. Metkar SS, Wang B, Ebbs ML, Kim JH, Lee YJ, Raja SM, et al. Granzyme B activates procaspase-3 which signals a mitochondrial amplification loop for maximal apoptosis. *J Cell Biol* 2003;160:875–85.
32. Kasai M, Yoneda T, Habu S, Maruyama Y, Okumura K, Tokunaga T. *In vivo* effect of anti-asialo GM1 antibody on natural killer activity. *Nature* 1981;291:334–5.
33. Nishikado H, Mukai K, Kawano Y, Minegishi Y, Karasuyama H. NK cell-depleting anti-asialo GM1 antibody exhibits a lethal off-target effect on basophils *in vivo*. *J Immunol* 2011;186:5766–71.
34. Obata K, Mukai K, Tsujimura Y, Ishiwata K, Kawano Y, Minegishi Y, et al. Basophils are essential initiators of a novel type of chronic allergic inflammation. *Blood* 2007;110:913–20.
35. Harshan KV, Gangadharam PR. *In vivo* depletion of natural killer cell activity leads to enhanced multiplication of Mycobacterium avium complex in mice. *Infect Immun* 1991;59:2818–21.
36. Zirger JM, Puntel M, Bergeron J, Wibowo M, Moridzadeh R, Bondale N, et al. Immune-mediated loss of transgene expression from virally transduced brain cells is irreversible, mediated by IFN γ , perforin, and TNF α , and due to the elimination of transduced cells. *Mol Ther* 2012;20:808–19.
37. Kennedy BC, Maier LM, D'Amico R, Mandigo CE, Fontana EJ, Waziri A, et al. Dynamics of central and peripheral immunomodulation in a murine glioma model. *BMC Immunol* 2009;10:11.
38. Kalos M, June CH. Adoptive T cell transfer for cancer immunotherapy in the era of synthetic biology. *Immunity* 2013;39:49–60.
39. Gajewski TF, Schreiber H, Fu YX. Innate and adaptive immune cells in the tumor microenvironment. *Nat Immunol* 2013;14:1014–22.
40. Wraith DC, Nicholson LB. The adaptive immune system in diseases of the central nervous system. *J Clin Invest* 2012;122:1172–9.
41. Alter G, Malenfant JM, Altfeld M. CD107a as a functional marker for the identification of natural killer cell activity. *J Immunol Methods* 2004;294:15–22.
42. Russell JH, Ley TJ. Lymphocyte-mediated cytotoxicity. *Annu Rev Immunol* 2002;20:323–70.
43. Bubenik J. MHC class I down-regulation: tumour escape from immune surveillance? (review). *Int J Oncol* 2004;25:487–91.
44. Zagzag D, Salnikow K, Chiriboga L, Yee H, Lan L, Ali MA, et al. Downregulation of major histocompatibility complex antigens in invading glioma cells: stealth invasion of the brain. *Lab Invest* 2005;85:328–41.
45. Kim W, Liau LM. Dendritic cell vaccines for brain tumors. *Neurosurg Clin N Am* 2010;21:139–57.
46. Bregy A, Wong TM, Shah AH, Goldberg JM, Komotar RJ. Active immunotherapy using dendritic cells in the treatment of glioblastoma multiforme. *Cancer Treat Rev* 2013;39:891–907.
47. Tobias A, Ahmed A, Moon KS, Lesniak MS. The art of gene therapy for glioma: a review of the challenging road to the bedside. *J Neurol Neurosurg Psychiatry* 2013;84:213–22.
48. Assi H, Candolfi M, Baker G, Mineharu Y, Lowenstein PR, Castro MG. Gene therapy for brain tumors: basic developments and clinical implementation. *Neurosci Lett* 2012;527:71–7.
49. Mohyeldin A, Chiocca EA. Gene and viral therapy for glioblastoma: a review of clinical trials and future directions. *Cancer J* 2012;18:82–8.
50. Simonato M, Bennett J, Boulis NM, Castro MG, Fink DJ, Goins WF, et al. Progress in gene therapy for neurological disorders. *Nat Rev Neurol* 2013;9:277–91.